

# **Preliminary characterization of the 40m radiotelescope at 22 GHz**

P. de Vicente

Informe Técnico IT-OAN 2008-8

## Revision history

<b>Version</b>	<b>Date</b>	<b>Author</b>	<b>Updates</b>
1.0	18-04-2008	P. de Vicente	First version

## Índice

<b>1. Introduction</b>	<b>3</b>
<b>2. General setup</b>	<b>3</b>
<b>3. Receiver-Backend setup description</b>	<b>4</b>
<b>4. Useful tools</b>	<b>5</b>
<b>5. Pointing model. First iteration</b>	<b>7</b>
<b>6. Focus determination</b>	<b>8</b>
6.1. Axial focus. First iteration . . . . .	8
6.2. Radial displacements and tilts of the subreflector . . . . .	10
6.3. Focus. Pointing effects . . . . .	13
<b>7. Pointing model. Second iteration</b>	<b>15</b>
<b>8. Efficiency, System temperature and SEFD</b>	<b>16</b>
<b>9. Open issues and pending tasks</b>	<b>19</b>

## 1. Introduction

This report describes the first results obtained during the commissioning of the 40m antenna. The pointing, focus and efficiency of the antenna at 22 GHz are reported here. The measurements were performed as part of the software development process. The author has written all the high level code that controls the antenna and the observations were part of this process since it allowed to test, debug and improve the code.

This report may seem incomplete but we had good reasons to leave it “unfinished”. High pressure was on the author to prepare the telescope for VLBI observations and there was no time to investigate the problems found while characterizing the telescope. Some of these issues, like systematic pointing errors, are still open at the time of the report and prevented to complete this task on a short time. A second report will be written once the pressure has disappeared and there is time to investigate and solve them. Open issues and pending tasks are summarized at the last section.

## 2. General setup

The geodetic coordinates for the 40m are reported by de Vicente (2005). Horizontal coordinates were obtained using an orthophotograph and referring them to the 14m antenna position derived from VLBI observations. The height was estimated from the topographic level curves, the height of the supporting tower and size of the receiver cabin and was also referred to the 14m antenna position. Since the 40m is a Nasmyth antenna, and its axis do not intersect, the coordinates refer to the point in the azimuth axis which is closest to the elevation axis. For completeness we reproduce the coordinates in table 1. These coordinates should be updated with those obtained from future VLBI observations.

Latitude (N)	Longitude (W)	Height (m)
40° 31' 28.87"	3° 05' 12.71"	989.9

Cuadro 1: 40m antenna geodetic position. Obtained using an orthophotograph and referred to the VLBI position of the 14 m antenna.

The pointing in elevation was corrected for refraction according to the algorithm described by Planesas et al. (2005). This model is applicable for elevations higher than 10 degrees. The refraction correction is done in real time from parameters collected at the weather station with a temporal periodicity of 1 minute. No observations were done with wind speeds higher than 5 m/s. Although the antenna designer, MT-Mechatronics, guarantees a non degraded operation for wind speeds higher than 10 m/s, we discovered that 8 m/s may have a non negligible impact in the pointing of the antenna depending on the relative orientation between the antenna and the wind direction.

The observations reported here were performed using the internal Heidenheim tables that the ACU uses. The inclinometers were not active and only one encoder in elevation was working. By the end of 2007 one of the two elevation encoders broke and by the time of this report a replacement was not installed yet.

### 3. Receiver-Backend setup description

After the basic tests on the servos of the 40m described elsewhere we have determined a pointing model, the dependency of the focus with elevation and the efficiency of the 40m antenna at 22 GHz.

The 22 GHz receiver is the first one installed at the 40m radiotelescope. It was installed initially in June 2007 and was used for the first radio detection performed by the 40m radiotelescope with the antenna stopped while a radio source (the moon) transited through the beam. The receiver was installed definitively at the beginning of 2008 and has been used since then for the commissioning of the antenna.

The 40m radiotelescope is a Nasmyth antenna and the radiation detected at the 22 GHz receiver reflects on 5 mirrors before arriving at the horn:

- M1. It is the main parabolic reflector.
- M2. It is an hiperbolic subreflector supported by a tetrapod and a structure at the end of it. This mirror has 5 degrees of movement: lateral displacements  $x$  and  $y$ , axial movement along  $z$  axis, and tilts around the  $x$  and  $y$  axis. The antenna can observe in primary focus or secondary focus. This is achieved by moving M2 along the parabola axis by 1 meter. The secondary position is achieved placing M2 in the closest position to the main reflector.
- M3. It is a planar rotating mirror along the parabola axis located at the receiver cabin and close to the focus of the antenna. This mirror has an elliptical shape since it always forms an angle of 45 degrees with the axis of the parabola. It moves synchronized with elevation such that it always points towards M2. Radiation arriving at M3 is directed perpendicular to the parabola axis. Two opposite directions can be selected, originating two branches of mirrors.
- M4'. It is a fixed planar mirror. It can be tilted 20 degrees and two positions are available:  $0^\circ$  and  $-20^\circ$ , but only the first one is used since the second one does not point to any receiver.
- M6. It is a fixed small parabolic mirror behind M5.

The 22 GHz receiver has two possible setups: VLBI and single dish, and two selectable bands: upper and lower band. Details are described by Malo et al 2006. For these tests we used the VLBI setup, the lower band and LCP (left circular polarization). In this configuration the receiver generates an instantaneous bandwidth of 500 MHz at the IF (Intermediate Frequency). The central frequency at the sky was 22580 MHz. Figure 1 shows a schematics for the 22 GHz receiver.

The signal is attenuated 22 dB at the FI output and sent through a YYY cable to the backends room where it is attenuated 19 dB further at the wideband continuum detector input. This detector, built at the Centro Astronómico de Yebes, (Gallego et al 19xx), has a bandwidth of 1150 MHz and generates an analog voltage which is read by a Keithely 2701 multimeter. The multimeter is remotely controlled and the values retrieved and stored on a FITS file together with information from the antenna. The chosen integration time for the observations described here was 1 second.

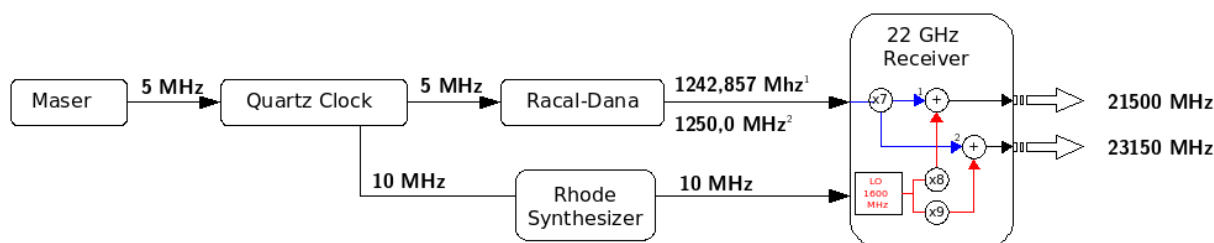


Figura 1: Setup frequency for the 22 GHz receiver

## 4. Useful tools

The search for a good pointing and focus behaviour can be accelerated with some useful tools which allow to know the behaviour of the radiotelescope in almost real time. These tools have also proved to be very valuable for the development and debugging of code, which was tested with these observations.

- KStars** KStars is a KDE application which renders the sky for any location and date on the Earth. It allows to command it from an outside application or script, by taking profit of DCOP. Using DCOP we can, for example, set the tracking center. On the other hand we can also define a FOV (Field Of View) symbol to represent the beamwidth of the 40m radiotelescope on the sky. These two features allow to display the antenna beam on the sky as the telescope moves. It is also possible to select interactively any zoom factor. The Python script below feeds KStars with its tracking position.

```

from Acspy.Common.Callbacks import *
import ACS, ACS__POA
import oanAcu40m, oanAcu40m__POA
from commands import *

# Using only the component and the properties:
#-----

sc = PySimpleClient()
c = sc.getComponent("BECKHOFF")

azimuth = c._get_actPosAz()
elevation = c._get_actPosEl()

kstarsInstance = getoutput("dcopfind -a 'kstars*'")

live = True

while (live):
az = azimuth.get_sync()[0]

```

```

el = elevation.get_sync()[0]
comando = "dcop %s KStarsInterface setAltAz %f %f" % (kstarsInstance, el, az)
salida = getoutput(comando)
kstarsInstance = getoutput("dcopfind -a 'kstars*')
if kstarsInstance != '':
    life = True
else:
    life = False

print "Finished..."
sc.releaseComponent("BECKHOFF")
sc.disconnect()

```

The beamwidth of the antenna can be created by selecting menu entry `Preferences->FOV symbols->Edit FOV symbols` and creating a new item. It is possible to choose a radio beam, by giving the diameter and observing wavelength. The zoom is controlled with the wheel of the mouse.

If the azimuth and elevation of the antenna are not updated frequently KStars, will show a jerky behaviour and the sources on the sky will apparently jump relative to the beamwidth. In the 40m antenna, at the time of this report, these values are updated each 250 ms, a too large value for KStars.

External catalogs can be imported and represented in the program, but versions below KDE 3.5.8 have an error that makes this feature useless. The author of this report is a collaborator of KStars and modified its code to fix that bug. The patched version was committed to the KDE SVN repository and is available for version 3.5.9. Versions 4.x use a different schema and this feature may work differently.

The format of the lines for a catalog is as follows:

```
0 09:03:53.15    67:57:22.686    3.704 J0903+679
```

The first column is the type of object, 0 means a point like one (like a star), second and third columns are Right Ascension and Declination at J2000, fourth column the magnitude and last column the source name.

Radio sources are characterized by their flux. The higher the flux, the brighter the source. KStars, as other similar applications represents sources according to their visual magnitudes. The lower the magnitude the brighter the source. In order to render radio sources on KStars and depict them with points with a size proportional to their flux, a catalog was created generating fake magnitudes between 2 and 7, assigning magnitude 2 to the largest flux and 7 the weakest on the catalog. This task was done by G. Quintana-Lacci as part of the elaboration of catalogs for the 40m antenna by Colomer et al.(2007).

When importing a catalog the user is given the possibility to choose a name for it, the color to represent all the sources it contains, and the order in which the columns with data appear. These settings are saved in a new file which will be loaded with each startup of KStars.

- **ACS Monitor** The last value obtained by the OAY-16 continuum detector may be monitored continuously, and represented graphically using a Java application from the ACS (Alma Common Software) infrastructure. This application may represent the last 500 hundred values and adjusts its scale either automatically or manually.

Running the previous two tools, KStars and the monitor, in separate windows it is possible to watch in real time at which relative position between the source and the antenna beam the maximum of the continuum radiation occurs. It is even possible to compare the detected intensity with the ones from previous scans if they are not too separated in time. This allows to correct the pointing of the antenna immediately after the scan has finished.

- **GILDAS** The analysis of the pointing needs to be done rigorously and for this we use GILDAS's single dish reduction program CLASS. GILDAS is installed in one of the computers. The details on how to interface it with ACS infrastructure and the telescope control system are out of the scope of this report and will be documented elsewhere.

## 5. Pointing model. First iteration

The determination for the pointing and focus model is an interactive process. In this section we describe the first step.

The starting point was to use the azimuth encoder offset determined from the preliminary pointing model for the optical telescope described by Alonso et al. (2008) to detect Jupiter. Elevation offset was determined by trial and error looking towards the moon. The antenna was pointed towards Jupiter and some single cross pointing drifts in azimuth and elevation were performed on top of it. Jupiter is the most intense almost point-like source in the sky at 22 GHz at the time of the report. The source can be approximated by a disk of constant intensity, with a size of  $36'' \times 34''$ , and a brightness temperature of 56.6 Jy.

Pointing scans were done close to the culmination, ( $180^\circ$  azimuth and  $27^\circ$  elevation). We used long arms of 20 arcmins to increase the possibility of detection. All these scans were done with the subreflector in its nominal central position. Figure 2 shows one of the first drifts taken on Jupiter by the 40 m. The HPBW was  $\simeq 75$  arcsecs. The intensity is in volts and no baseline was removed.

Next step was to determine a preliminary pointing model for the 40 m by using the first azimuth and elevation pointing offsets and following Jupiter from the culmination to the horizon. We adjusted the pointing manually. There was a small dependence of the pointing with elevation and no significative dependence on the azimuth angle.

Once we had an approximate idea of pointing at low elevations we tried to make pointing drifts while tracking 3C84. 3C84 is one of the brightest quasars at 22 GHz, although its flux is variable and it culminates close to the zenith in the Centro Astronómico de Yebes, since its declination is very similar to the latitude of the observatory. The azimuth for 3C84 only varies 30 degrees from its rise time until it reaches an elevation of 75 degrees and therefore it is an excellent candidate to determine the elevation pointing error versus elevation without much influence from the azimuth angle and azimuth collimation errors.

Pointing drifts on 3C84 were done from 15 degrees elevation up to 80 degrees elevation. We

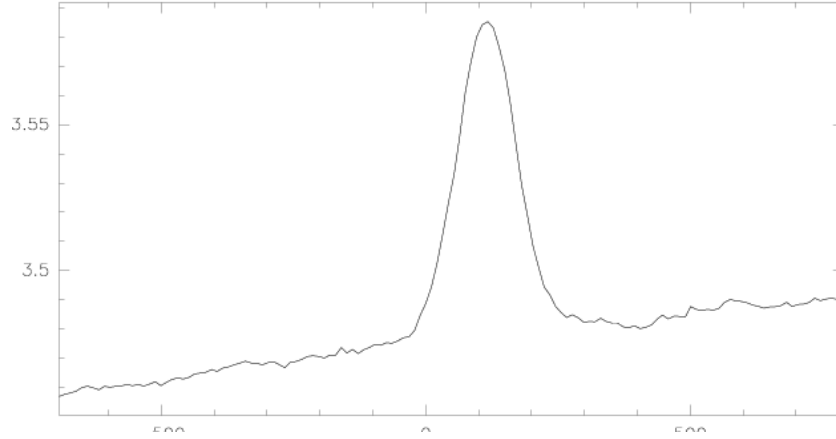


Figure 2: Azimuth drift on Jupiter. Intensity scale is in volts. HPBW is  $80''$  approximately. The baseline was not removed

used arms 1024 arcsecs in length. During the whole sequence we corrected manually the pointing. At high elevations the pointing correction for the azimuth encoder was higher indicating a collimation error for the receiver. Figures 3 and 4 show azimuth pointing errors and elevation pointing errors versus elevation.

With a very poor coverage of the sky we obtained a clear idea of the azimuth and elevation encoder offsets, the azimuth collimation error and the gravitational effect on elevation errors. These errors are described by  $P_1$ ,  $P_2$ ,  $P_7$ ,  $P_8$  and  $P_9$ , which were determined using the previous plots and fitting manually a function to them. Our first pointing model guess was:

$$P_1 = 2570'' \quad P_2 = 120'' \quad P_7 = -460'' \quad P_8 = 0'' \quad P_9 = -280''$$

These values were tested later making pointing drifts on quasars at different locations of the sky. Errors were always below 40 arcsecs. This model was used to determine the focus of the antenna.

## 6. Focus determination

### 6.1. Axial focus. First iteration

An axial displacement of the focus is along the Z axis, which ideally should coincide with the paraboloid and hiperboloid axis. It causes a change in the intensity of the detected signal and a widening of the beam width of the antenna (Baars 1973). Therefore the best axial focus is determined by measuring the intensity at different focus positions and at different elevations. This is only possible once we had an acceptable pointing model.

Axial focus determination was achieved making several pointing crosses at different Z values of M2. The drifts were shorter than those used for pointing in order to last less time and have similar elevations at the different Z values. Each series was made with 5 or 6 different positions of the focus, with a total displacement of 2 wavelengths (24 mm).

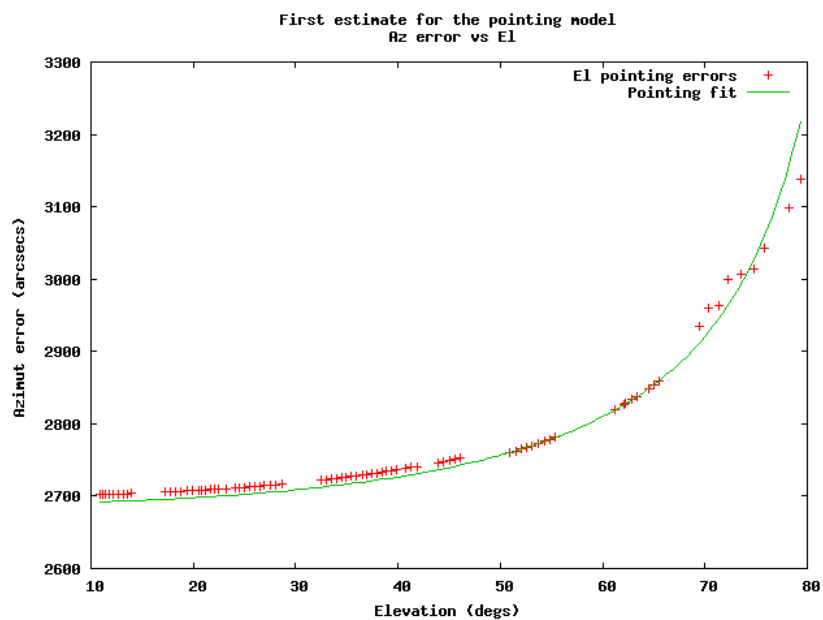


Figura 3: Preliminary fit to match collimation error in azimuth. Encoder offset used:  $2570''$ , Collimation error:  $120''$ .

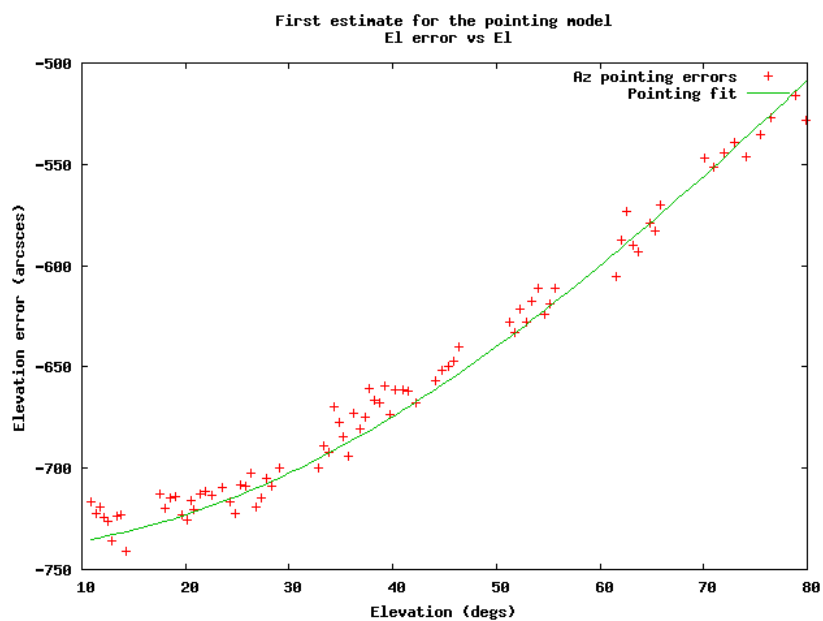


Figura 4: Preliminary fit to match gravitational deformation as function of elevation. Cosine function with a constant term  $-460''$  and an amplitude of  $200''$ .

The final results are visible in Figure 5 where we represent the best Z position from 10 to 80 degrees. The more negative the value, the larger the distance between the main reflector and the subreflector. The total displacement of the focus from 0 to 90 degrees according to this measurement is 27 mm, which probably is due to the gravitational pull and the homologous design of the antenna, that modifies its shape changing the focus position.

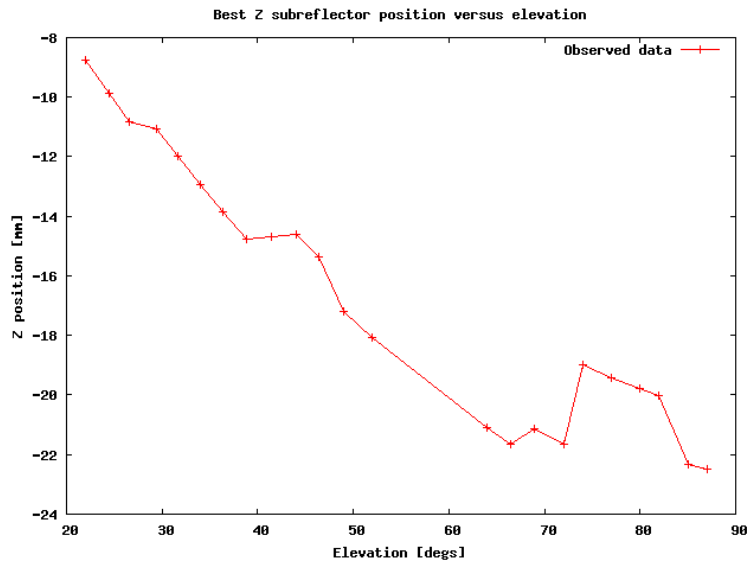


Figure 5: First Z focus fit versus elevation.

This result was improved once we determined X and Y positions of the subreflector and we had a better pointing model. Final results are reported in figure 6.

## 6.2. Radial displacements and tilts of the subreflector

Lateral displacements of the subreflector cause asymmetries in the beam, like coma, small decrease of the antenna gain and a pointing change which depends on the geometry of the antenna. Beam asymmetries require a large dynamic range to avoid secondary lobes being masked by noise. We performed some observations at Jupiter’s culmination, where elevation and azimuth change slowly, and at different elevation using galactic source DR21.

Figures 7 and 8 show vertical and horizontal cuts of the beam on Jupiter at an elevation of 26 degrees. The main effects of the subreflector radial displacement, asymmetry, gain decrease and a pointing error, can be easily seen.

The best Y position for the subreflector at 27 degrees elevation is +12 mm and the best X position -6 mm.

Figures 9 and 10 show vertical and horizontal cuts of the beam on DR21 at an elevation of 80 degrees. As with Jupiter, the main effects of the subreflector radial displacement can also be seen. From the figures, one can conclude that the best subreflector X position is  $\simeq$  -6 mm.

The Y position of the subreflector varies from 12 mm at 27 degrees elevation to -30 mm at 80 degrees elevation. This means that the subreflector apparently “falls” along the Y axis when

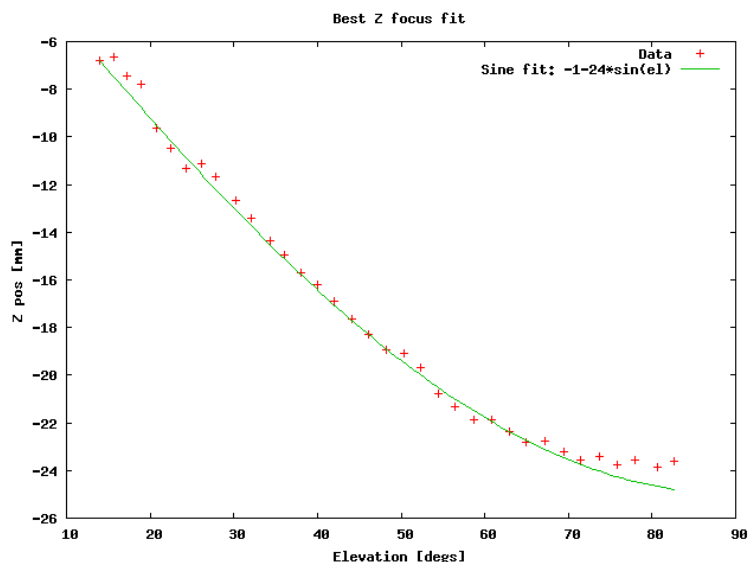


Figure 6: Final fit to Z focus versus elevation. This new focus was fit after X and Y focus were already determined.

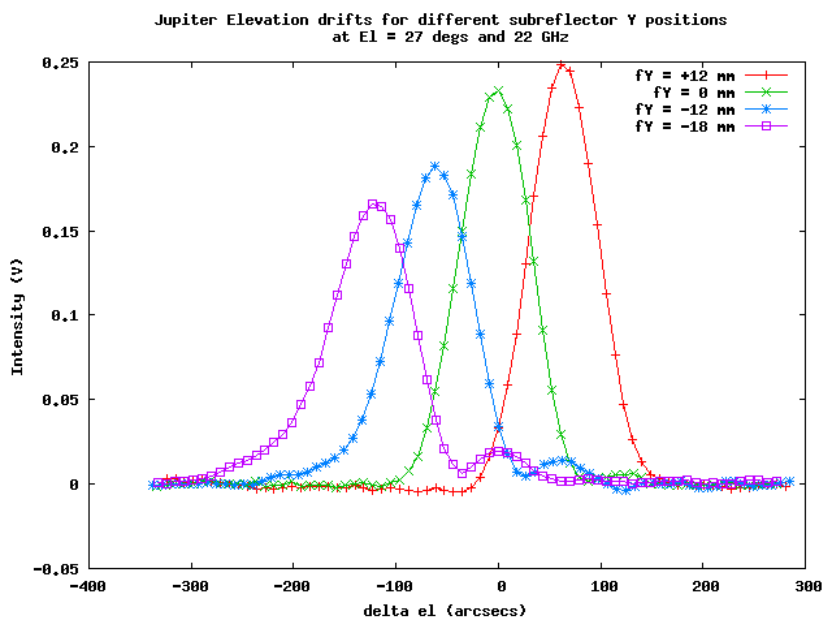


Figure 7: Vertical cut of the antenna beam at 22 GHz with different Y positions of the subreflector. The cut was obtained making elevation drifts around 26 degrees elevation on Jupiter. The pointing change due to the displacement of the subreflector was not corrected. Hence the main lobe is located at a different position.

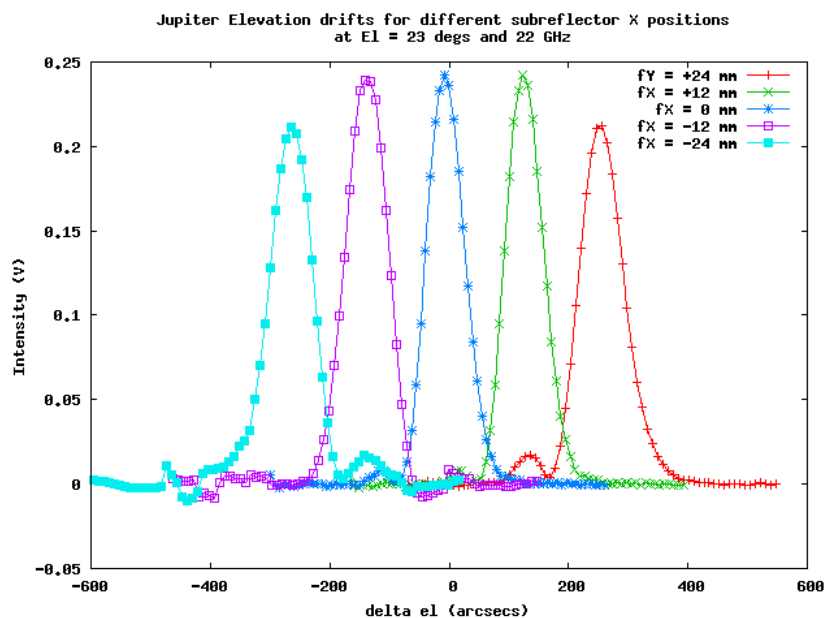


Figure 8: Horizontal cut of the antenna beam at 22 GHz with different X positions of the subreflector. The cut was obtained making azimuth drifts around 25 degrees elevation on Jupiter. The pointing change due to the displacement of the subreflector was not corrected. Hence the main lobe is located at a different position.

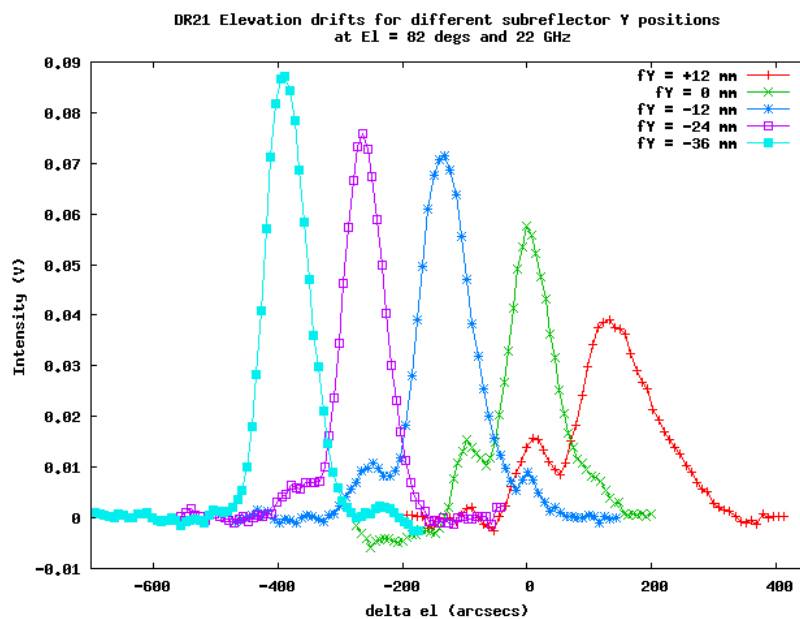


Figure 9: Vertical cut of the antenna beam at 22 GHz with different Y positions of the subreflector. The cut was obtained making elevation drifts around 82 degrees elevation on DR21. In this case the pointing change due to the displacement of the subreflector was corrected and hence the main lobe is centered in the scan.

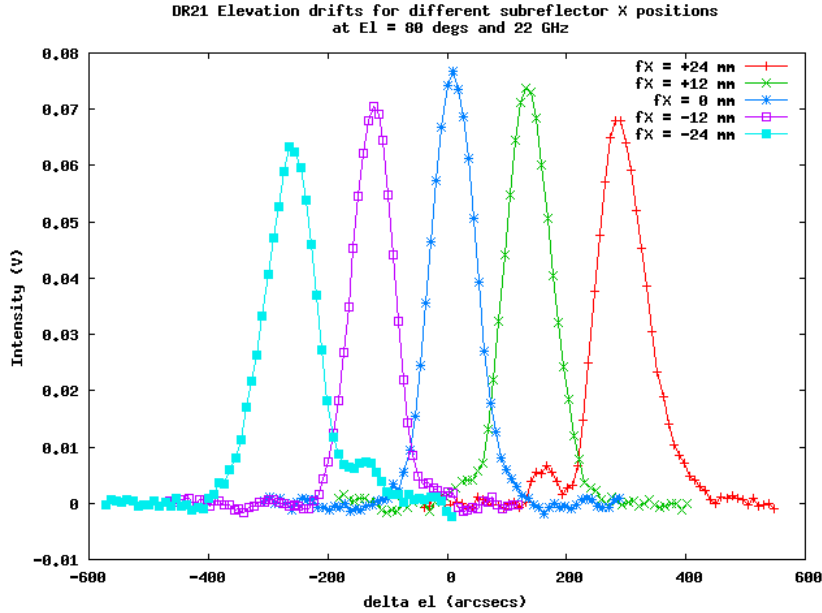


Figure 10: Vertical cut of the antenna beam at 22 GHz with different  $Y$  positions of the subreflector. The cut was obtained making elevation drifts around 82 degrees elevation on DR21. In this case the pointing change due to the displacement of the subreflector was corrected and hence the main lobe is centered in the scan.

the antenna is tilted towards the horizon. The most probable explanation is that the tetrapod support legs suffer a gravitational flexure, as it happens with a cantilever with one free end. We have investigated the behaviour of the subreflector along the  $Y$  axis by making drifts on cuasar 3C84 and on DR21. The result is shown in figure 11. We have fitted a cosine function to the data. Our best fit is:

$$y [\text{mm}] = -40 + 60 \cos(el) \quad (1)$$

where  $el$  is the elevation.

The subreflector shows a constant shift in the  $X$  axis, which does not depend on the elevation. Figure 12 depicts the intensity ratio between the secondary lobes and the main lobes at 25 and 75 degrees elevation for 5 different  $X$  values of the subreflector nominal center. A parabola can be fitted to the five points of each series. The maximum of the parabola is located at  $-6$  mm.

### 6.3. Focus. Pointing effects

We have also investigated the effect of the movements of the subreflector in the pointing of the antenna. Displacements of the subreflector in  $X$ , and  $Y$  and tilts around  $X$  and  $Y$  cause a pointing change. The pointing changes were obtained by fitting a line to 5 different positions of the subreflector for each of the 4 cases. Table 2 summarizes the pointing errors due to a change of position of the subreflector.

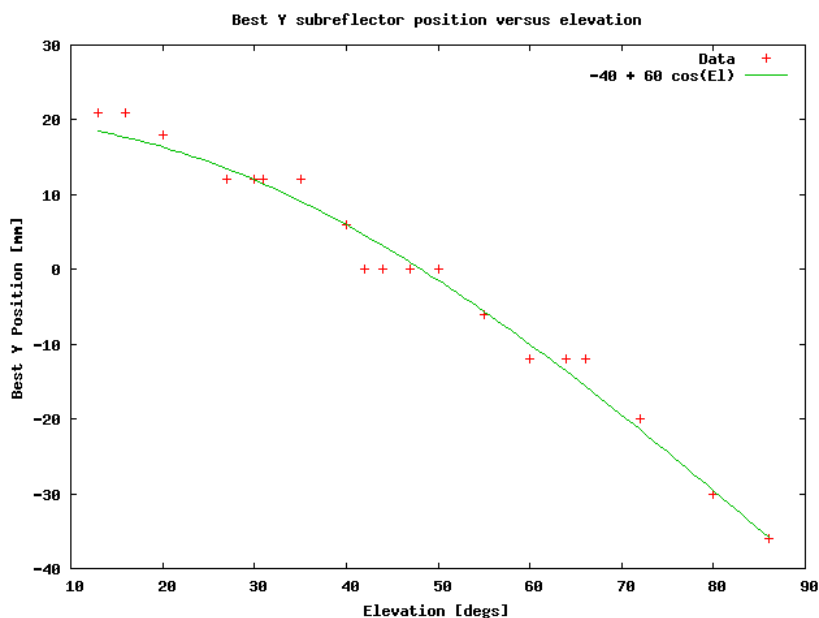


Figure 11: Best subreflector position along Y versus elevation. Values were obtained making pointing drifts on 3C84 and DR21. The resolution is limited by the wavelength and it is not possible to determine it better than 6 mm.

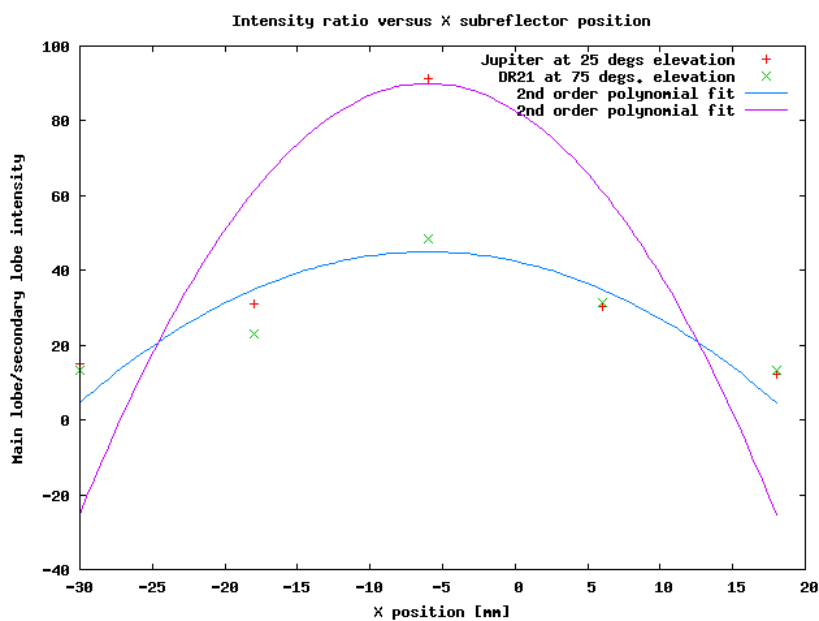


Figure 12: Main lobe secondary lobe intensity ratio at different elevations for different X subreflector positions. Values were obtained making pointing drifts on Jupiter (25°) and DR21 (75°). The resolution is limited by the wavelength and it is not possible to determine it better than 6 mm. The best value is  $X = -6$  mm

Subreflector change	Units	Col Az error (arcsecs)	El error (arcsecs)
X displacement	1 mm	11	0
Y displacement	1 mm	0	11
Tilt around X	1 arcsec	0	0.150
Tilt around Y	1 arcsec	-0.150	0

Cuadro 2: Pointing errors due to radial displacements and tilts of the subreflector.

Surprisingly we have also noticed that Z focus displacements cause a pointing error. Figures 13 and 14 show a series of pointing scans on 3C84. Each block of the series was performed with 5 different Z positions. The series was done while tracking the source from horizon to the zenith. We can see a saw effect, which indicates a clear dependence of the pointing on the Z focus.

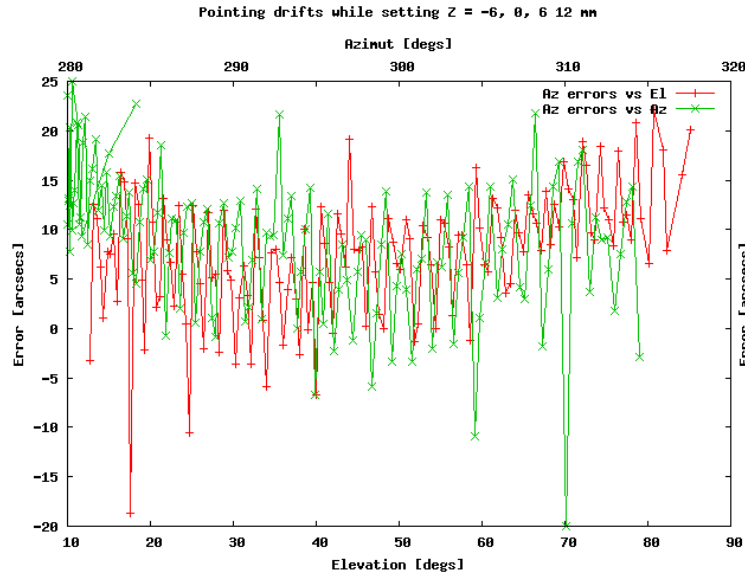


Figure 13: Azimuth and elevation error versus azimuth for 3C84 while periodically changing Z from -6 to 12 mm in steps of 6 mm.

## 7. Pointing model. Second iteration

After applying the focus corrections for Y and X the starting pointing model had to be modified to take into account these effects (see table 2.  $X = -6$  mm position for M2 causes a collimation pointing error in azimuth of 66 arcsecs. Equation 1 yields a correction of  $-440''$  for  $P_7$  and  $660''$  for  $P_9$ .

Hence the new model parameter were:

$$P_1 = 2570 \quad P_2 = 120 - 66 = 54 \quad P_7 = -460 - 440 = -900 \quad P_8 = 0 \quad P_9 = -280 + 660 = 380$$

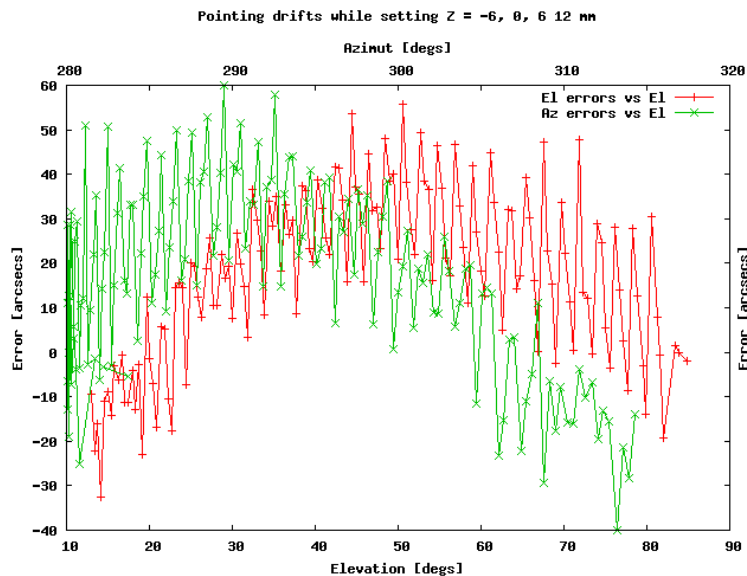


Figura 14: Azimuth and elevation error versus elevation for 3C84 while periodically changing Z from -6 to 12 mm in steps of 6 mm.

We tested this model on 5 different sources: Jupiter, Venus, DR21, 3C84, J1642+398, J2253+161 and the pointing error was better than 15 arcsecs all over the sky. We tried to determine the results with a pointing fit program and unfortunately this was unsuccessful since the solution did not converge.

## 8. Efficiency, System temperature and SEFD

We have estimated the efficiency of the antenna versus elevation despite the current pointing errors and focus uncertainties. Figure 16 shows the normalized gain versus elevation but the result should be taken with caution and as preliminary estimation since pointing errors may affect the results. The gain drops towards high elevations.

The efficiency of the antenna was obtained at  $\sim 60$  degrees elevation using 3C84. By the end of february, the source was 11.3 Jy (private communication). To convert from voltages to antenna temperature (K) we placed a hot and cold load in front of the 22 GHz horn and detected the signals with the wideband OAY 14 continuum detector. Table 3 summarizes the system temperatures determined. Calibration was 29 K/Volt. The maximum detected voltage was 0.11 volts which corresponds to  $\sim 3.2$  K.

Hot temperature voltage ( $V_{hot}$ ) and cold temperature voltage ( $V_{cold}$ ) are:

$$\begin{aligned} V_{hot} &= K(T_{hot} + T_r) + V_0 \\ V_{cold} &= K(T_{cold} + T_r) + V_0 \end{aligned}$$

where  $T_{hot}$  is the cabin temperature and  $T_{cold}$  is the cold load temperature (usually 70 K). The

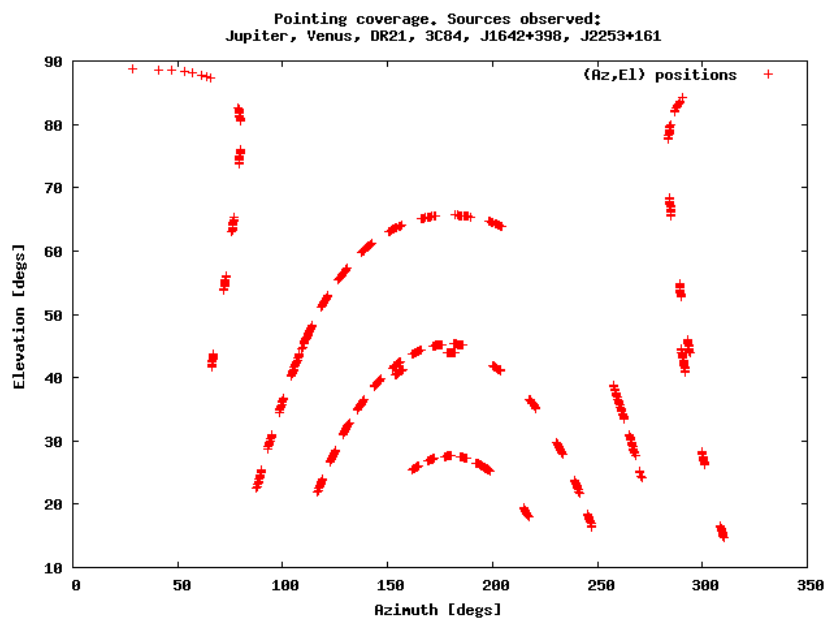


Figure 15: Pointing coverage. Observations were performed between March 28th and April 3rd 2008. Observed sources: Jupiter, Venus, DR21, 3C84, J1642+398, J2253+161

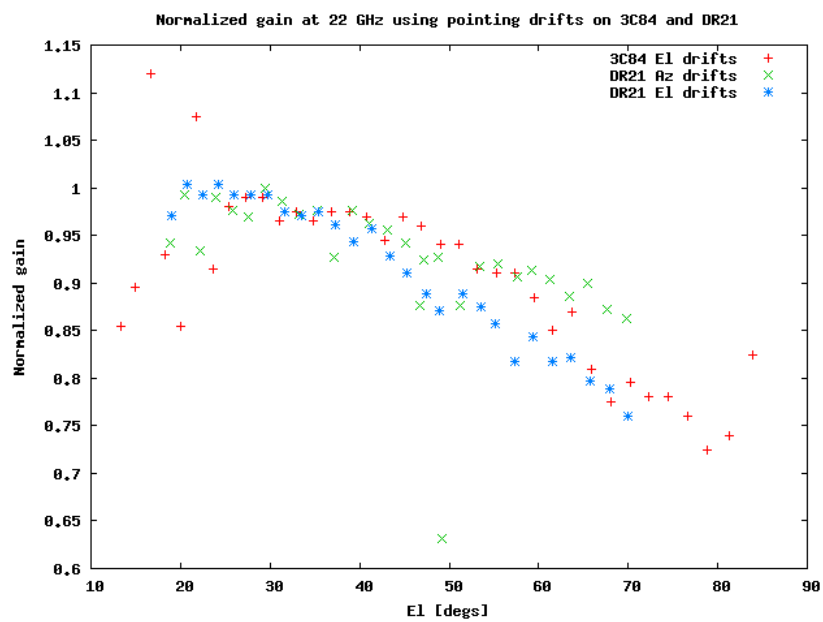


Figure 16: Normalized gain obtained observing DR21 and 3C84. Efficiency is  $\sim 0,5$  at the peak (see the text below in this section).

Cabin Temp. (C)	Pol.	Hot Temp. Voltage	Cold Temp Voltage	T <sub>receiver</sub>
287.9	LCP	10.902	3.547 V	31 K
288.0	RCP	10.896	3.435 V	25 K

Cuadro 3: Data obtained on 27/3/2008, previous to characterizing the CAL diode. The polarization here corresponds to the receiver, and does **not** match the one at the sky since radiation is reflected in an odd number of mirrors.

receiver temperature is:

$$T_r = \frac{T_{hot}V_{cold} - T_{cold}V_{hot}}{V_{hot} - V_{cold}}$$

The zero of the continuum detector was setup to be of the order of a few millivots and hence negligible. From the previous table we get a K/volt ratio of 26.5 K/volt. This ratio is only valid while the attenuators and gains are kept at the same level and cease to be valid if they change. The maximum 3C84 detected voltage was 0.11 volts which corresponds to  $\sim 2.9$  K.

The flux/antenna temperature ratio depends on the antenna aperture efficiency:

$$\eta_a = \frac{2K_B T_a}{A_g S_f \exp(-\tau A)} C_s^{-1} = 2,197 \frac{T_a [\text{K}]}{S_f [\text{Jy}]} C_s^{-1} \quad (2)$$

where  $K_B$  is the Boltzmann constant,  $A_g$  is the antenna area (40m diameter),  $T_a$  the antenna temperature,  $S_f$  the source flux,  $\tau_a$  the atmospheric opacity,  $A$  the number of air masses from zenith, and  $C_s$  is a factor which depends on the source brightness distribution,

$$C_s = \begin{cases} 1 + x^2 & \text{gaussian source} \\ \frac{x^2}{1 - \exp(-x^2)} & \text{disk source} \end{cases} \quad (3)$$

where,

$$x = \frac{\theta(\prime\prime)}{\text{HPBW}(\prime\prime)} \quad (4)$$

Since 3C84 is point like compared to the HPBW, we have assumed  $C_s = 1$ . If we neglect opacity:

$$\eta_a = 2,197 \text{ Jy/K} \frac{2,9\text{K}}{11,3\text{Jy}} = 0,56 \quad (5)$$

However we can also suppose opacity is 0.07 at 22 GHz at zenith which amounts  $\sim 1.07$  at 60 degrees elevation:

$$\eta_a = 2,197 \frac{2,9 \exp(0,07 / \sin(el))}{11,3} \simeq 0,60 \quad (6)$$

The RMS of the surface can be estimated assuming that the aperture efficiency depends on the blockage ( $\eta_b$ ), the illumination (taper plus spillover) ( $\eta_i$ ) and the RMS of the reflector:

$$\eta_a = \eta_b \eta_i \eta_{RMS} \quad (7)$$

The blockage was estimated by de Vicente (1998) and it is supposed to be 0.92. The illumination efficiency is 0.78 (private communication from F. Tercero). Hence:

$$\eta_{RMS} = \frac{\eta_b \eta_i}{\eta_a} = \frac{0,60}{0,92 \cdot 0,78} = 0,84 \quad (8)$$

According to the Ruze formula the RMS of the surface relates to the efficiency as:

$$\eta_{RMS} = \exp(-(4\pi\sigma_{rms}\lambda)^2) \quad (9)$$

and

$$\sigma_{rms} = \frac{\sqrt{-\ln(\eta_{RMS})}}{4\pi/\lambda} \quad (10)$$

$$= 430\mu m \quad (11)$$

System temperature was measured at 3 different elevations and results are summarized in table 4:

Elevation (°)	Polarization	T <sub>sys</sub>
89	RCP	52 K
45	RCP	58 K
15	RCP	88 K

Cuadro 4: System temperature obtained on 27/3/2008, previous to characterizing the CAL diode.

SEFD is determined from the T<sub>sys</sub> temperature and the antenna temperature (which strongly depends on the efficiency):

$$SEFD = S_f \frac{T_{sys}}{T_a} \quad (12)$$

From 3C84 antenna temperature (2.9 K) and a T<sub>sys</sub> of 58 K at 45°:

$$SEFD = 11,3 \frac{58}{2,9} = 226 \text{ Jy} \quad (13)$$

All the previous numbers are too uncertain to be definitive and should be rechecked with different calibrators, an accurate model for the atmosphere opacity and skydips. They are reported here as a preliminary estimate.

## 9. Open issues and pending tasks

The following issues should be addressed in a future report regarding the 40m behaviour at 22 GHz.

- One of the most important pending problems is the different pointing errors obtained when the antenna tracks a source from zenith to the horizon (downwards) than from the horizon to the zenith (upwards). This behaviour can be seen in figure 17 which shows elevation errors obtained from pointing drifts on 3C84 from the zenith towards the horizon and immediately after on DR21 from the horizon to the zenith. Errors may differ as much as 40 arcsecs for the same elevation. Azimuth is different for both sources but this error was checked by pointing on the same source at mid elevation and moving the antenna from upwards and from downwards.

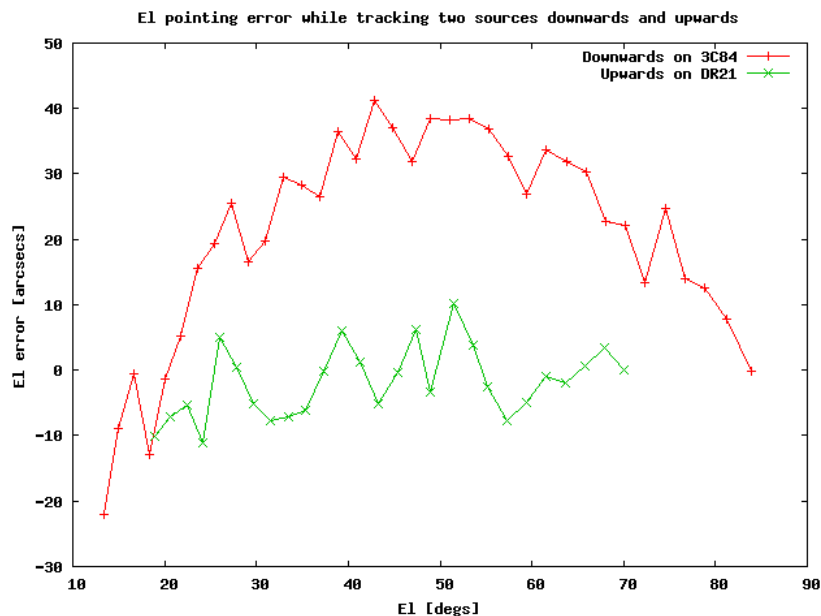


Figure 17: Elevation errors obtained from elevation drifts on 3C84 (downwards) and DR21 (upwards). The drifts were done with a Z focus value that maximized the intensity of the signal.

- The lack of convergence when using a pointing program to solve for the pointing model should be studied carefully. This lack of convergence is possibly associated to the problem described in the previous item. It might be possible that problems with pointing are mitigated after the installation of the second encoder.
- The pointing change as a function of an axial displacement (along Z) of the subreflector should be studied deeply once the previous item is solved.
- We have observed jumps in the detected power while making drifts for determining the focus and pointing of the 40 m. Figure 18 shows an example. We have not identified whether this detected power changes are due to interferences or to gain changes in the receiving chain. No easy correlation between the antenna position and the presence of jumps has been observed.
- Skydips should be performed at different frequencies and good weather conditions to determine the opacity and forward efficiency of the antenna.

- Amplitude calibration should be revisited once the CAL diode temps are provided along the observing band.
- The error pattern, beam shape and main beam efficiency should be determined.

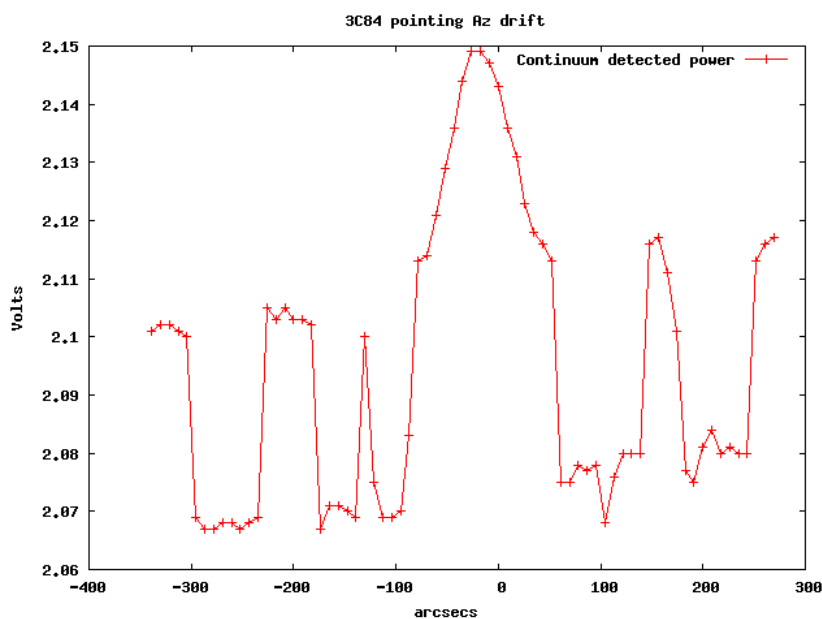


Figura 18: Example of erratic intensity jumps for a horizontal drift on 3C84 taken on 24-03-2008 at an azimuth of 78 degs and elevation of 69.4. Intensity is in volts.

## Referencias

- [1] J. W. M. Baars. IEEE Trans. Antennas Propag., Vol. AP-21, p. 461 - 474, 1973.
- [2] P. Planesas. "Corrección por refracción atmosférica para el radiotelescopio de 40m del CAY". IT-OAN 2003-2
- [3] P. de Vicente. "Eficiencia por bloqueo en un paraboloide. Antena de 40 m.". IT-OAN-1998-10.
- [4] P. de Vicente. "Nuevo emplazamiento de la antena GPS en el CAY". IT-OAN-2005-9
- [5] P. de Vicente, R. Bolaño, L. Barbas. "Primera prueba con el sistema de control del radiotelescopio de 40m. Observaciones". IT-OAN 2007-8
- [6] P. de Vicente. "Deconstructing a pointing model". IT-OAN-2008-27
- [7] I. Malo, J.A. López Fernández, M. Azuaga, J. Fernández. "Medidas del Receptor de 22 GHz". IT-OAN 2006-4

- [8] J.D. Gallego, , A. Barcia, J. E. Garrido. "Diseño construcción y características del convertor OAY 09 para el terminal VLBA del C.A.Y." IT-OAN-1993-2